# FABRICATION OF TRANSPARENT POLYMER NANOCOMPOSITES CONTAINING PMMA-GRAFTED CeO$_2$ PARTICLES

**A Thesis Submitted to**
**the Graduate School of Engineering and Sciences of**
**İzmir Institute of Technology**
**in Partial Fulfillment of the Requirements for the Degree of**

**MASTER OF SCIENCE**

**in Chemistry**

**by**
**Onur PARLAK**

**May 2011**
**İZMİR**

We approve the thesis of **Onur PARLAK**

**————————————————**

**Assoc.Prof.Dr. Mustafa M. DEMİR**
Supervisor

**————————————————**

**Prof.Dr. Serdar ÖZÇELİK**
Committee Member

**————————————————**

**Assist.Prof.Dr. Aylin Ziylan ALBAYRAK**
Committee Member

**20 May 2011**

**————————————————**                    **————————————————**

Prof.Dr. Serdar **ÖZÇELİK**                    Prof.Dr. Durmuş Ali **DEMİR**
Head of the Department of Chemistry        Dean of the Graduate School
                                            Engineering and Sciences

# ACKNOWLEDGEMENTS

# ABSTRACT

## FABRICATION OF TRANSPARENT POLYMER NANOCOMPOSITES CONTAINING PMMA-GRAFTED $CeO_2$ PARTICLES

The composite materials prepared by transparent polymer and nanosized particles possess promising future in optical design and applications since their controllable optical properties. In this study, transparent/translucent composite films based on polystyrene (PS) and poly(methyl methacrylate) (PMMA)-grafted $CeO_2$ nanoparticles were prepared. $CeO_2$ nanoparticles were precipitated from $Ce(NO_3)_3 \cdot 6H_2O$ and urea in dimethyl formamide at 120°C. The surface of the nanoparticles was modified with a polymerizable surfactant, 3-methacyloxypropyltrimethoxy silane (MPS) in situ at 0°C. The size of the particles was fixed to 18 nm in diameter. The particles were dispersed into a mixture of MMA:toluene solution. The free radical solution polymerization was carried out in situ at 60°C using benzoyl peroxide (BPO) as initiator. A PMMA layer is formed around $CeO_2$ nanoparticles. The thickness of the shell ranged from 9 to 84 nm was controlled by the amount of BPO using 6 and 0.5 wt %, respectively with respect to monomer. The layer thickness was found to be inversely proportional with the amount of initiator. The resulting PMMA-grafted $CeO_2$ particles were blended with PS in tetrahydrofuran and the solution was spin-coat on a glass slide. $CeO_2$ content in the composite films was fixed to 5.5 wt %. The transmission of the films was examined by UV-vis spectroscopy. The transmission of the PS composite prepared by neat $CeO_2$ particles was 71 %. It was increased to 85 % when the composite prepared with PMMA-grafted $CeO_2$ particles whose PMMA thickness is 9 nm. We believe that the achievement in transparency is most probably due to the reduction in refractive index mismatch between $CeO_2$ particles and PS matrix using PMMA layer at interface.

# ÖZET

## PMMA KAPLANMIŞ CeO$_2$ TANECİKLERİ İÇEREN ŞEFFAF POLİMER NANOKOMPOZİTLERİN ELDESİ

Şeffaf polimerler ve nanoboyutta parçacıklardan oluşan kompozit malzemeler sahip oldukları kontrol edilebilir optik özelliklerinden dolayı optik tasarımlarda ve uygulamalarda umut vaadeden bir geleceğe sahiptir. Bu çalışmada, polistiren (PS) ve polimetil metakrilat (PMMA) kaplanmış CeO$_2$ nanotaneciklerryle hazırlanmış şeffaf/yarı şeffaf kompozit filmler elde edilmiştir. CeO$_2$ nanotanecikleri, dimetil formamid içerisinde hazırlanan Ce(NO$_3$)$_3$·6H$_2$O ve ürenin 120 °C' de çöktürülmesi ile elde edilmiştir. Nanoparçacık yüzeyleri polimerleşebilen bir yüzey aktifleştirici olan 3-metakriloksipropiltrimethoksisilan (MPS) ile 0 °C'de tepkime ortamında değiştirilmiştir. Tanecikler, boyutları 18 nm olacak şekilde hazırlanmıştır. Tanecikler MMA:toluen karışımı içerisinde dağıtılmıştır. 60 °C' de benzoil peroksit (BPO) başlatıcısı varlığında serbest radikal polimerleşmesi gerçekleştirilmiştir. Parçacıkların etrafında PMMA tabakası oluşturulmuştur. Parçacık üzerindeki polimer kabuğun kalınlığı monomere göre kütlece % 6 'dan % 5' e kadar değişen oranda BPO kullanarak 9 nm' den 84 nm' ye kadar kontrol edilmiştir. Polimer tabakasının kalınlığının başlatıcının miktarı ile ters orantılı olduğu gösterilmiştir. Elde edilen PMMA kaplı CeO$_2$ parçacıkları tetrahidrofuran içerisindeki PS ile karıştırılmış ve cam üzerine döngü kaplama ile kaplanmıştır. Kompozit film içerisindeki CeO$_2$ miktarı kütlece % 5.5 oranında hazırlanmıştır. Filmlerin optik iletimi UV-vis spektrometresi ile incelenmiştir. Yüzeyi değiştirilmemiş CeO$_2$ parçacıkları ile hazırlanmış PS kompozitlerinin optik iletimi % 71 olarak bulunmuştur. Yüzeyi 9 nm kalınlığında PMMA tabakası ile kaplanmış CeO$_2$ parçacıkları ile hazırlanan kompozitte ise optik geçirgenlik % 85' e çıkarılmıştır. Şeffaflıkta elde edilen bu iyileşmenin sebebinin, CeO$_2$ ile PS arasındaki kırılma indisi uyumsuzluğunu azaltan ara yüzeydeki PMMA tabakası olduğu düşünülmektedir.

# TABLE OF CONTENTS

# LIST OF FIGURES

# LIST OF TABLES

# CHAPTER 1

# INTRODUCTION

## 1.1. Nanoparticle  Polymer Composites: A Smart Association

The combination of nanoparticles with polymers to generate composite materials has been experienced for many years. The early examples date back to the middle of 19th century. Charles Goodyear, who was also inventor of vulcanized rubber attempted to prepare nanoparticle-reinforced automobile tires by blending carbon black, zinc oxide and magnesium sulfate with a rubber. (Balazs, et al. 2006; Goodyear 1856) Although a little wiggling  was perceived in the early of 1900's by the the invention of clay-reinforced resin known as Bakelite, (Baekeland 1909) a long period of time, scientific community fallen a deep sleep about this topic until the early 1990's. In the 1993, a group of scientist from Toyota company succeeded to produce five-fold strengthen nylon by blending with mica. (Balazs, et al. 2006; Kojma 1993) After that time, many researches have been successively performed and eventually this research area in material science has been refreshed. From that time on, thousands of combinations have been tried in both academic and industrial researches. According to the Web of Science Database (Data were collected by the time at 23.04.2011), when some related words are searched for in topic, following data were obtained. The numbers represent number of publications in related search topics.

Polymer composites: 30.570

Polymer nanocomposites: 13.156

Nanoparticle polymer nanocomposites: 3.571

Optical properties of nanoparticle polymer nanocomposites: 462

From the beginning of 1970's to early of 1990's, average number of publications per year on polymer composites is only 21, however from 1990's to 2011, that number increases 72-fold and reaches to 1507 publications per year. While polymer nanocomposites constitute  43 % of all polymer composite studies,

nanoparticle polymer nanocomposites constitute only 12 %. Moreover, optical properties of nanoparticle polymer nanocomposites constitute only 1.5 %. Based on these data, it is obviously seen that, studies on optical properties of nanoparticle polymer composites are very scarce and it can be said that ''There is still plenty of room at the bottom.''

To design polymer nanocomposites, a lots of material such as carbon nanotubes, inorganic nanoparticles, clay minerals, and biomaterials have been used for two decades to improve mechanical, thermal, transport, and optical properties. (Bockstaller, et al. 2005; Bombalski, et al. 2007; Tu, et al. 2010) Recently, optical applications of polymer nanocomposites come into prominence in parallel with the development of optic, optoelectronic, information, and telecommunication technologies. The composites prepared by a transparent polymer and nanosized pigment particles have attracted great interest since they exhibited controllable optical properties. (Beecroft and Ober 1997; Caseri 2009; Lu and Yang 2009) Polymers, on the one hand, offer transparency, ease of processing, and structural flexibility; pigment particles, on the other hand, provide desired features including high refractive index, emission, absorption, nonlinear optical properties. By combination of these two dissimilar materials, material scientists have long appealed to develop novel optical polymer nanocomposites for various existing and potential applications such as waveguides, (Chang and Chen 2002; Yamada, et al. 1999; Yoshida and Prasad 1996) liquid crystal display coating, (Qi and Hegmann 2008) and non-linear optical materials. (Asunskis, et al. 2008; Du, et al. 2002; Elim, et al. 2003; Feng, et al. 2009; Kulyk, et al. 2009; Yuwono, et al. 2006) To this aim, many pigment particles and transparent polymers have been associated. Some examples are ZnO/PMMA, ZnO/PHEMA, (Hung and Whang 2005) $SiO_2$/PMMA, (Palkovits, et al. 2005) $TiO_2$/PVAL, (Nussbaumer, et al. 2003) CdS/PS, (Du, et al. 2002) CdS/PMMA, (Khanna and Singh 2007) $ZrO_2$/PMMA, (Hu, et al. 2009)¸ CdTe/PS, (Zhang, et al. 2003) $BaTiO_3$/PI. (Devaraju, et al. 2005) However, a sharp refractive index increase at the interface of pigment particles and polymer matrix results strong scattering, thereby optical clarity of the composite system rapidly diminishes.(Hulst) Rayleigh scattering that is applicable to small, dielectric (non-absorbing), and spherical particles has been mainly applied. Based on this theory, when the size of scatter is smaller than the wavelength of incident light, light scattering is suppressed and the medium remains transparent. Moreover, the intensity of scattering increases with the radius of the scatterer and with the mismatch in refractive index of

scatterer and surrounding medium. The loss of transmitted light intensity by scattering can be estimated by the following expressions: (Caseri 2006; Novak 1993)

$$T = \frac{I}{I_0} = \exp\left[-\frac{3\phi r^3}{4\lambda^4}\left(\frac{n_p}{n_m}-1\right)\right]s \qquad (1.1)$$

$$T = \frac{I}{I_0} = \exp\left[-\frac{32\pi^4\phi_p\chi r^3 n_m^4}{\lambda^4}\left[\frac{\left(n_p/n_m\right)^2-1}{\left(n_p/n_m\right)^2+2}\right]^2\right] \qquad (1.2)$$

where $T$ is the transmission, $r$ is the radius of scatteres, $\lambda$ is wavelength, $\phi$ is particle content, $s$ or $x$ is thickness of the material investigated, $n_p$ and $n_m$ are the refractive indices of the particles and the polymer matrix, respectively. Among the four parameters, the size of the scatterers is obviously the dominant one. (Caseri 2009) A slight increase in the radius of scatters causes a dramatic decrease in the intensity of incident beam and makes the material rapidly opaque.
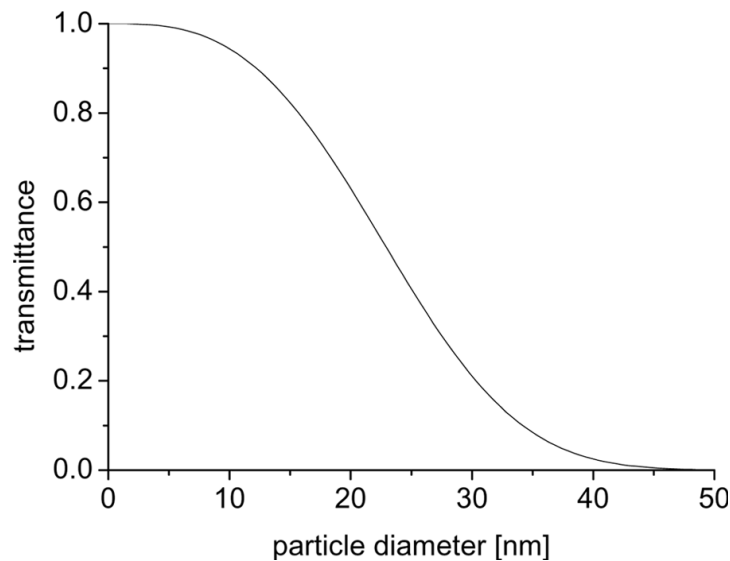


Figure 1.1. Transmittance of composite of 100 μm thickness, volume fraction of particles of 0.1, refractive index of the matrix of 1.5 and of the particles 2.7 at a wavelength of 500 nm calculated with Equation 2. (Source: Caseri, et al. 2009)

Scatterers here refer to particle domains. A particle domain could be an individual particle or an aggregate/agglomerate of many individual nanoparticles. Considering the strong tendency of nanosized particles forming large particle domains,

the achievement of transparency in polymer nanocomposites is quite demanding. This is because an intensive work in literature has been focused on to control the domain size of nanosized pigment particles in preparation of transparent nanocomposites. For the size of optically isotropic particles is significantly is less than wavelength of the light, the particle cross-section is formulated by the following expressions: (C.F. Bohren 1983)

$$C_{sca} \approx \left[ V_p \left( \Delta \alpha \right) \right]^2 \qquad (1.3)$$

Where $V_p$ is the particle volume and $\Delta \alpha$ is the polarizability of the particle in polymer matrix.

$$\left| \Delta \alpha \right| \approx \left( \left( \varepsilon_p - \varepsilon_m \right) / \left( \varepsilon_p + 2 \varepsilon_m \right) \right) \gg 0 \qquad (1.4)$$

Where $\varepsilon_p$ and $\varepsilon_m$ are dielectric constants of the particles and polymer matrix respectively and it is expressed as ($\varepsilon_i = (n_i)^2$). For the most of inorganic-polymer materials combination, even if the particles are in range of 20-40 nm and non-aggregated, the scattering cannot be prevented and transparency of nanocomposites still remains an inadequate.(Demir, et al. 2007b)

The physical origin of scattering is the refractive index (RI) mismatch between particles and surrounding polymer matrix.(Hulst) When RIs of the components match, light cannot differentiate particles as a scatteres, and eventually scattering can be prevented, at least to some extends.(Schulz, et al. 2007) RI is an intrinsic property; however, it can be readily modified by the addition of a second material component which can modify the RI of the materials such that the mismatch between particles and polymer matrix can be minimized. Based on this approach, scattering of inorganic particles can be suppressed by grafting of polymer/different inorganic phase of correct composition, molecular weight and/or shell thickness from the surface of particles. Grafting of particle surface allows one to match the effective dielectric constant of the desired core-shell particle to the dielectric constant of the embedding medium. For the core-shell particles at wavelengths larger than particle diameter, dielectric constant, in other words, refractive index of filler particles can be calculated by Maxwell-Garnett theory as

$$\varepsilon_{eff} = \varepsilon_{shell}\left(1 + 3\frac{\phi\chi}{1 - \phi\chi}\right) \qquad (1.5)$$

where $x = 1/3(\varepsilon_{core}-\varepsilon_{shell})/(\varepsilon_{core}-\varepsilon_{shell}))$, $\varepsilon_{core}$ and $\varepsilon_{shell}$ represent the dielectric constant of the particle core and shell respectively. $\phi = V_{core} / (V_{core} + V_{shell})$ is the relative particle core volume.(Bombalski, et al. 2007) With this approach, when the effective dielectric constant of the integral filler particle equals to the embedding medium, scattering can be suppressed. Equation 5 allows one to match refractive index of filler particles and embedding medium by the following condition ($n_{particle} > n_{medium} > n_{shell}$).

Recent progress in the fabrication of well-defined nanostructured(Advincula 2006; Talapin, et al. 2010) and binary mixture of oxidic particles have allowed to engineer the refractive index of the filler particles.(Schulz, et al. 2005; Yang, et al. 2008) Bockstaller and Matyjazewski showed the reduction of optical scattering of $SiO_2$ nanoparticles in toluene.(Bombalski, et al. 2007) A PS layer was obtained on the surface commercial $SiO_2$ nanoparticles with 0.19 weight percentage of $m$(PS) relative to $m$($SiO_2$) using surface-initiated Atom Transfer Radical Polymerization. The scattering coefficient of the resulting core-shell particles is reduced more than 20 folds compared to that of neat $SiO_2$ nanoparticles. According to the Authors' word, a null scattering condition is achieved with this material combination.
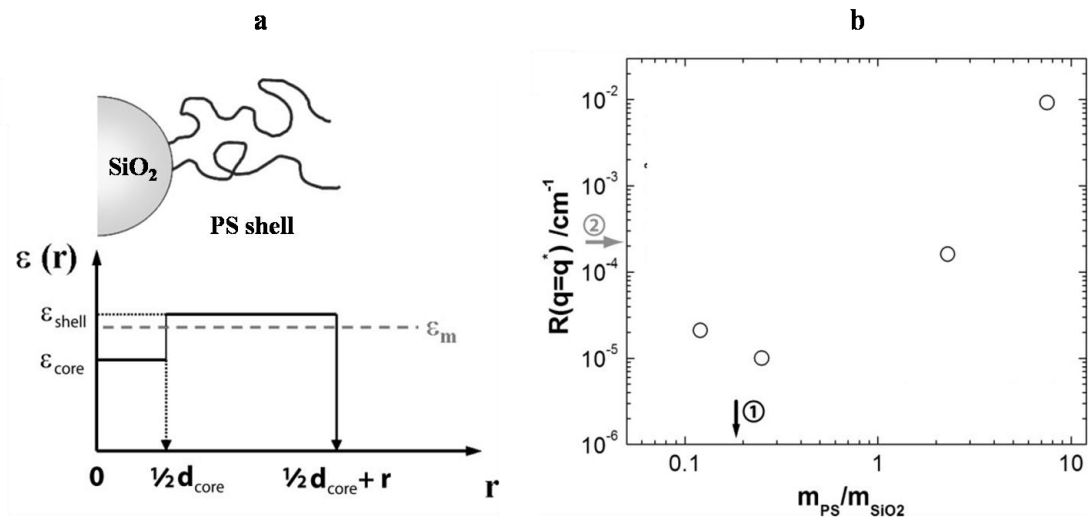
Figure 1.2. Proposed design for core-shell particles (a), change in scattering intensity as a function of particle composition. (Source: Bombalski, et al. 2007)

Another example using index matching approach to achieve transparency was reported by Li et al. (Li, et al. 2008) The core–shell structured silica–titania nanoparticles were prepared and embedded into transparent epoxy matrix. The transmittance of particle loaded epoxy composites was investigated as a function of mass composition $m(TiO_2)/m(SiO_2)$. A variety of weight percent of shell was prepared on silica core ranging from 0 to 60 wt %. For loading of 1 wt % of core-shell particles, it was claimed that the optimal transmittance of the nanocomposite was attained at a the shell content where refractive index matching is satisfied between core-shell particles and polymer matrix.(Li, et al. 2008)
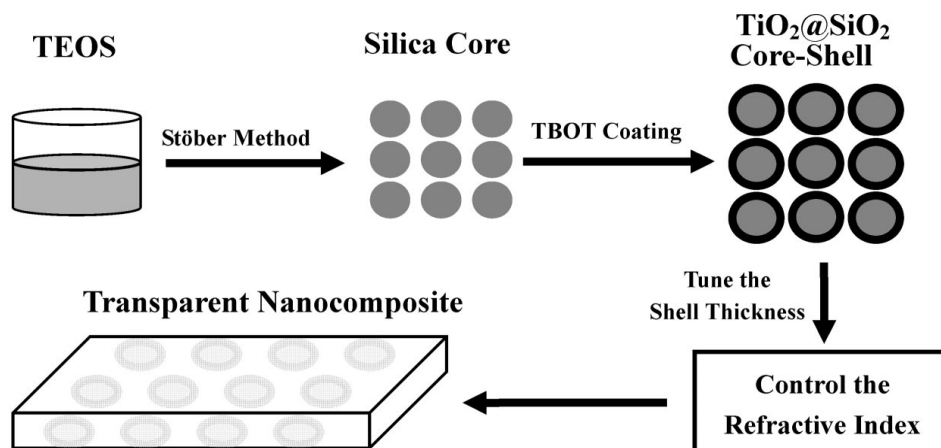


Figure 1.3. Schematic illustration for the preparation of the transparent S-T/epoxy nanocomposites.(Source: Li, et al. 2008)
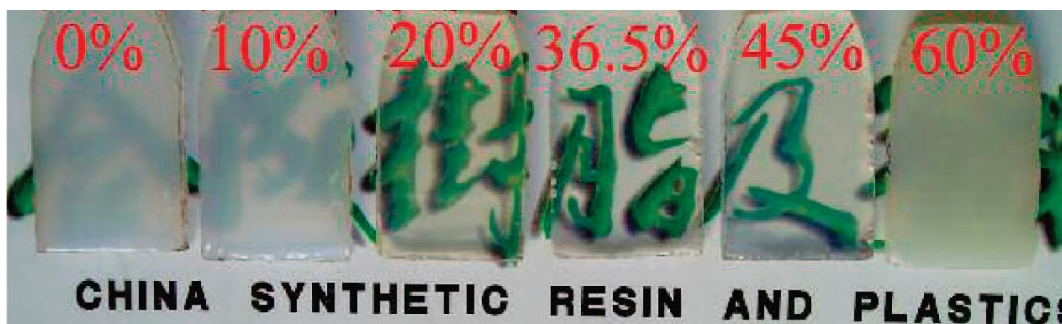
Figure 1.4. Photo of nanocomposites as a function of the shell weight percentage.
(Source: Li, et al. 2008)

Mixed-oxide nanoparticles are also utilized for the preparation of transparent nanocomposites by index matching principle mainly used in dental applications. Silica fillers are widely used in composites structure because of their well-studied silanization mechanisms resulting in excellent polymer/filler particles. It is a good host for heavy metals centers. It has no absorption band at all in the visible spectrum and has refractive index at 1.46 at 633 nm. The addition of heavy metals into $SiO_2$ structure such as $Ta_2O_5$ (Schulz, et al. 2005) or ZnO (Yang, et al. 2008) enables to control the refractive index of mixture and provides transparency of the polymer nanocomposites. The refractive index of these particles can be controlled via the heavy metal oxide component. For $SiO_2/Ta_2O_5$ system, RI was changed from 1.46 ($=SiO_2$) to more than 1.8. In the present work, we demonstrated that transparency of a composite system can be remarkably increased when refractive index difference is minimized between particles and surrounding polymer matrix. The association of PS and unmodified $CeO_2$ particles result an opaque material due to the both aggregation of particles and the RI mismatch. A robust and facile procedure for the preparation of translucent system taking PS matrix and PMMA-grafted $CeO_2$ is proposed as a model system. Ceria is a wide band-gap semiconductor and absorbs in UV-A region of optical spectrum and emits light in wavelength.(Zhang, et al. 2004) It has a refractive index 2.20 at 633 nm.(D.N.) PS and PMMA are two transparent and incompatible polymers.(Helfand and Tagami 1972) The indice of surrounding PS matrix is 1.59.(J. C. Seferis in : J. Brandrup) The mismatch in refractive indices between matrix and nanoparticles is offset by PMMA layer, whose index is 1.49 at the same wavelength.(J. C. Seferis in : J. Brandrup) This layer is found with a controlled thickness on the ceria employing free radical solution polymerization.

This combination of materials ($n_{CeO2} > n_{PS} > n_{PMMA}$) fulfills index matching principle when the correct composition of CeO$_2$ and PMMA is provided.

# CHAPTER 2

# PREPARATION TRANSPARENT PS / PMMA-GRAFTED CeO₂ NANOCOMPOSITES

Optical bulk nanocomposites based on polystyrene and PMMA-grafted $CeO_2$ collaidal nanocomposite particles were prepared. The schematic demonstration of the entire process is presented in Figure 2.1. In the following, synthesis and chracterization of each step of this process are discussed in detail.
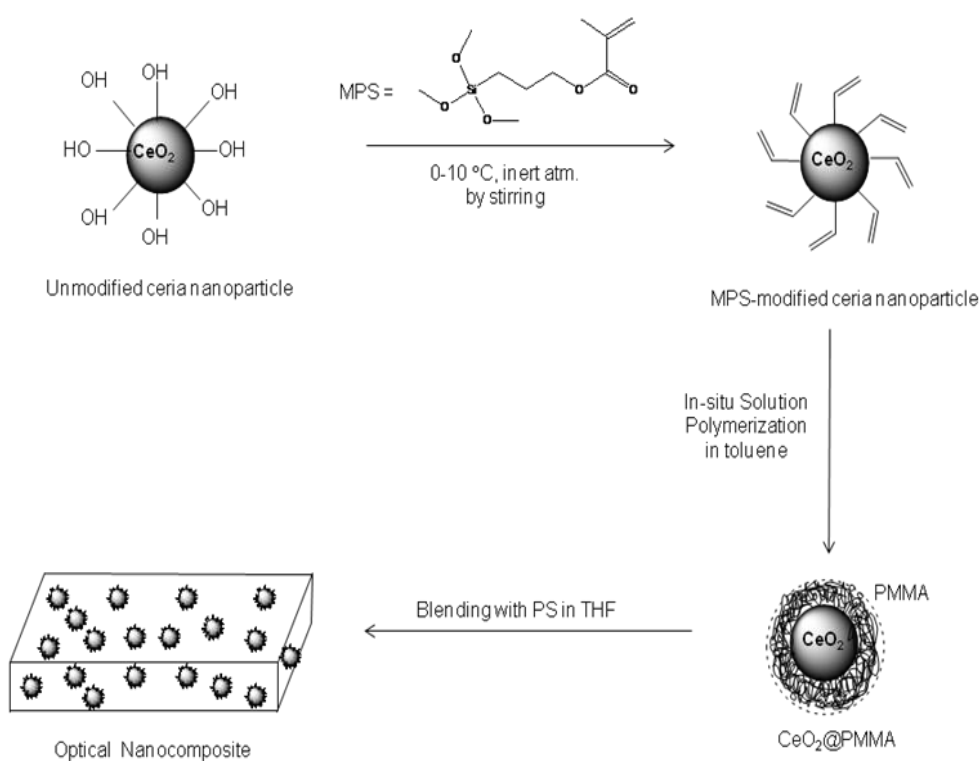


Figure 2.1.   Schematic illustration for the preparation of transparent PS / PMMA-grafted CeO₂ nanocomposites.

## 2.1 Experimental

## 2.1.1 Synthesis and Surface Modification of CeO$_2$ Nanoparticles

Nanosized ceria (CeO$_2$) particles were precipitated from solution of Cerium nitrate hexahydrate (Ce(NO$_3$)$_3$·6H$_2$O) and urea (CO(NH$_2$)$_2$) in dimethyl formamide (DMF). In a typical run, 12.5 mL of 1.5 M urea solution was dripped at a rate of 2-3 mL·min$^{-1}$ from a syringe into an equal volume of 0.5 M Ce(NO$_3$)$_3$·6H$_2$O solution at 120 °C, then refluxed under mild stirring. Reflux was maintained for 1h. For surface modification of nanosized CeO$_2$ particles, 0.5 mL of MPS in 5 mL DMF was injected dropwise to the above suspension under nitrogen atmosphere at 0-10 °C. The mixture was then further stirred for 12 h. The resulting suspensions were subjected to three cycles of centrifugation to isolate the CeO$_2$ nanoparticles. The particles were washed with fresh ethanol to remove excess MPS and were dried in a vacuum at 50 °C for 8 h prior to *in situ* polymerization.
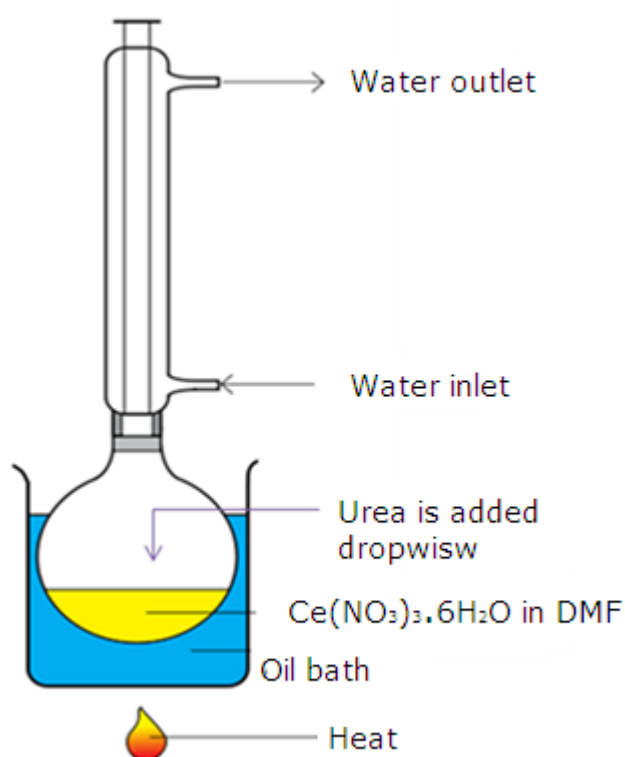


Figure 2.2. Schematic illustration CeO$_2$ nanoparticle synthesis.

## 2.1.2. Preparation of PMMA-grafted $CeO_2$ Core-shell Particles

The surface-modified $CeO_2$ particles (20.0 mg) were dispersed in a mixture of MMA-toluene (10:20 in mL). The polymerization was carried out in the presence of these particles at 60 °C using BPO as initiator with different contents (0.5, 1.0, 1.5, and 2.0, 4.0, 6.0 wt % ). The particle content was fixed to 0.1 wt % with respect to the amount of MMA. The dispersions in MMA-toluene mixture were sonicated for 15 min and kept overnight in the dispersed state to provide complete wetting of particle surface. After a second sonication for 15 min, BPO was added into each dispersion with different amounts. Three cycles of a freeze-thaw process were applied to the dispersions prior to polymerization. The flask containing surface modified ceria particles and MMA/toluene mixture were placed into a preheated oil-bath at 60 °C. The polymerization proceeded under nitrogen atmosphere along 6 h, and it was ended up by quenching to room temperature. The resulting colloidal nanocomposite particles ($CeO_2$ core-PMMA shell) were isolated by three cycles of centrifugation and washing with THF were used to remove unreacted monomer and free polymers in the polymerization mixture. Then, the colloidal nanocomposite particles were dried in vacuum at 40 °C for 12 h.

## 2.1.3. Preparation of PS / PMMA-grafted $CeO_2$ Nanocomposite Films

$CeO_2$ core-PMMA shell particles were dispersed in PS-THF solution ( 20.0 wt % PS ), and kept overnight in the dispersed state by stirring. For each dispersion, $CeO_2$ content was kept constant (5.0 wt %). After sonication for 30  min, composite films were prepared by spin-coating (Laurell Technologies Corp.) on glass or quartz substrates. The film thickness was controlled by the variation of solid content of the THF solution and by the spinning speed.

## 2.2. Results and Discussion

## 2.2.1. Controlled Precipitation of Ceria Nanoparticles

Nanosized $CeO_2$ particles were prepared by the precipitation of $Ce(NO_3)_3 \cdot 6H_2O$ and urea in DMF at 120 °C. $Ce(NO_3)_3 \cdot 6H_2O$ was dissolved in preheated DMF and urea was gradually added into the solution under continous stirring. At the beginning of the reaction, the mixture was clear. After 15 min of reaction, it turned into translucent indicating that nucleation of $CeO_2$ particles started. In 1h reaction time, the mixture turned into opaque dispersion. Average size of particles was followed by DLS during the reaction and it was found that size of particle increased gradually up to the submicron levels at the end of 6h. Figure 2.3. shows average particle size after 1 hour is 18 nm. When the reaction was proceeded for further 5 hours, average diameter of particles reaches 600 nm. Because of that, monitoring of particle size against time was crucial to designate the surface modification time.
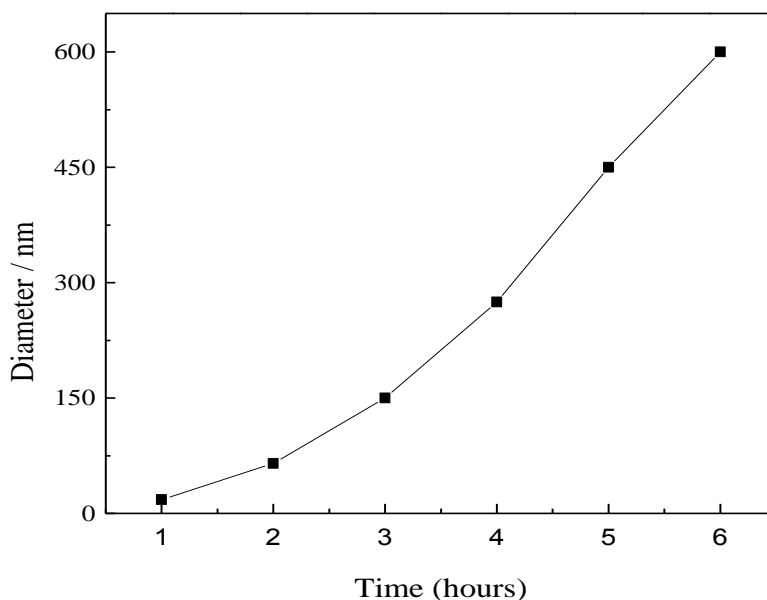


Figure 2.3. Particle diameter *versus* time of the $CeO_2$ particles in reaction medium.

While the particles grow and simultaneously new particles nucleated, a polymerizable surfactant (3-methaxcryloxypropyl trimethoxysilane) (MPS) was added into the dispersion at 1h reaction time. The reactor was quenched to 0-10 °C to prevent

polymerization of the surfactant at high temperature. This in situ surface modification was proceeded for further 12 hours to achieve a uniform surface coverage. Particle size was followed by DLS and it was found that the MPS-modified $CeO_2$ particles were kept 18 nm in diameter. MPS as a surfactant has dual functions: (i) stabilization of particle dispersion and make particles redispersible in organic medium. (ii) provide suitable environment to generate polymer layer on particle surface due to the presence of vinyl groups. To validate particle stabilization after surface modification, MPS-modified and unmodified $CeO_2$ particles were redispersed in DMF and size of particles was measured after 12 days aging. After a period of 12 days at room temperature, average diameters of MPS-modified particles were found to be still 18 nm. However, size of unmodified particles increased to the 850 nm due to the agglomeration of particles. Figure 2.4. shows change in average diameters of both modified and unmodified particles after 12 days. Inner image of Figure 2.4. also shows appearance of each dispersion. It was seen that, dispersion containing modified ceria were still clear.
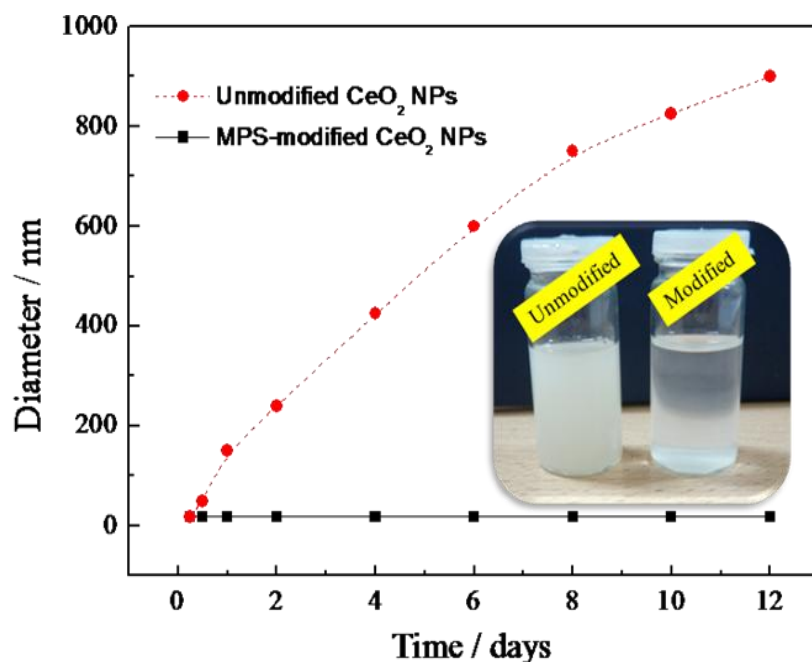


Figure 2.4. Particle diameter versus aging time of the $CeO_2$ particles in DMF.

To characterize bonding fashion of MPS on $CeO_2$ particles, ^{1}H NMR spectra of the polymerizable surfactant (MPS), unmodified $CeO_2$ particles and MPS-modified $CeO_2$ particles in deutorated dimethyl sulphoxide (DMSO-$d_6$) were measured. In the

spectrum of MPS, the resonance signals at 6.01 and 5.64 ppm may belong to the methylene protons ($H_1$); and the signals at 4.03, 1.67 and 0.62 ppm are attributed to the α-$CH_2$, β-$CH_2$, γ-$CH_2$ protons ($H_3$, $H_4$ and $H_5$) to methacrylate respectively. The signal at 1.87 ppm is caused by methyl protons near the methylene group ($H_2$). The most intense signal at 3.46 ppm is due to the presence of nine methyl protons on the trimethoxysilanes in the same environment ($H_6$). Unmodified $CeO_2$ particles does not give any specific resonance signal. In the spectrum of unmodified $CeO_2$, the resonance signal at 3.30 ppm may belong to the surface hydroxyl (-OH) protons on the particle surface. However, in the spectrum of MPS-modified particle, all signals belongs to MPS is still observed. The sign of chemical grafting of MPS on to the particle surface can be observed by line broadening. In signal coming from methylene protons (-$OCH_3$) at 3.40-3.46 is broadened after MPS modification to the surface of particles. (Kohlmann, et al. 2001)
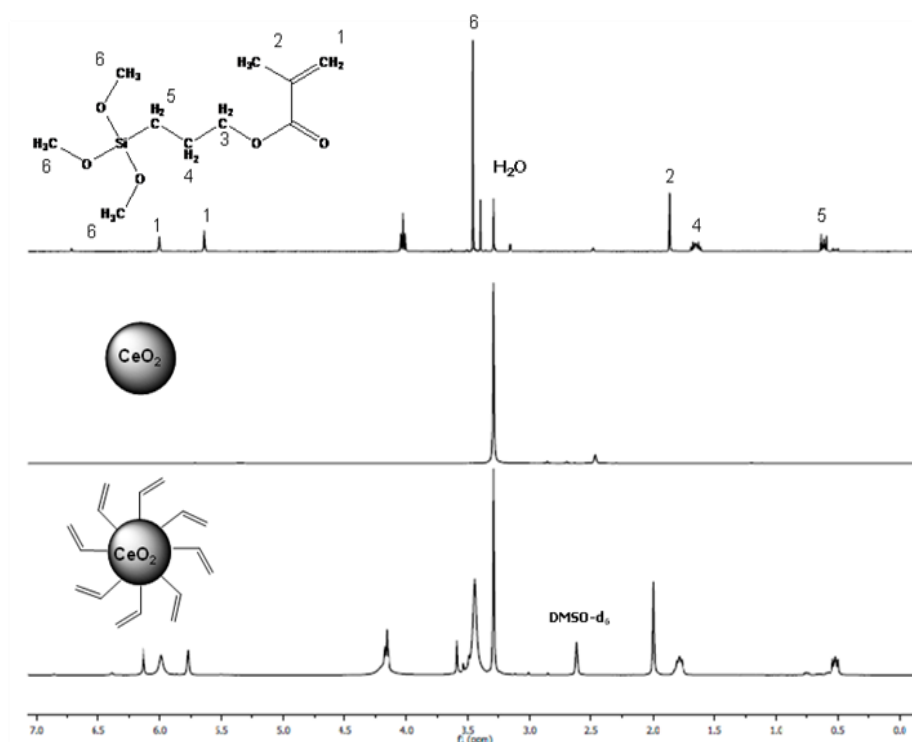


Figure 2.5. $^1$H NMR spectra of the polimerizable surfactant, unmodified $CeO_2$ nanoparticles and MPS-modified nanoparticles.

## 2.2.2. Preparation of PMMA Layer on the Ceria Nanoparticles

The MPS-modified particles were dispersed into a mixture of MMA-toluene and polymerization was carried out in situ at 60 °C using BPO as an initiator. The vinyl groups on the particles surface are reactive and contribute to polymerization of MMA. Eventually, the particles are covered with a PMMA layer. The PMMA-grafted $CeO_2$ colloidal nanocomposites were isolated by dissolution of bulk polymer in the reaction using THF and by centrifugation to be further dispersed into bulk PS matrix. Interparticle distance must be longer than the size of the average chain. If an average polymer chain gets longer than interparticle distance during polymerization, the chain may transit more than one particle. As a result, a three dimensional network where particles are junction points is formed throughout reactor and the particles cannot be isolated from the system by dissolution since crosslinked structures are insoluble. This is because the particle content in the in situ polymerization is an important point that must be carefully adjusted. It was fixed to low content (0.1 wt %) to prevent formation of undesirable network structure.

Figure 2.6. presents the number size distribution of MPS-modified and PMMA-grafted $CeO_2$ hybrid particles prepared at different BPO content. The results were obtained by DLS in toluene. While MPS-modified $CeO_2$ particles exhibit uniform size distribution with a mean diameter of 18 nm, the size of PMMA-grafted $CeO_2$ hybrid particles extends to large diameters depending on the amount of BPO employed. The diameter of the hybrid particles was found to be inversely proportional with BPO content. For example, the mean diameter of the hybrid particles was 36 nm when the amount of BPO was 6 wt %. As BPO content was reduced to 0.5 wt %, the mean of the particle size distribution increased gradually to 186 nm. PMMA-grafted $CeO_2$ particles hybrid particles are, in fact, have core-shell nanostructure. The diameter of $CeO_2$ core was kept at 18 nm and PMMA shell varied depending on initiator content. Assuming that the core particles have spherical shape and a uniform grafting of PMMA chains exist, PMMA shell thickness (*t*) can be obtained by subtracting the diameter of $CeO_2$ core than the mean diameter of PMMA-grafted $CeO_2$ particles. The left-y-axis of Figure 2.7. shows the thickness of PMMA layer estimated by this subtraction as a function of initiator (BPO) at fixed amount of monomer. The thickness showed a first order decay with increasing of the initiator content.
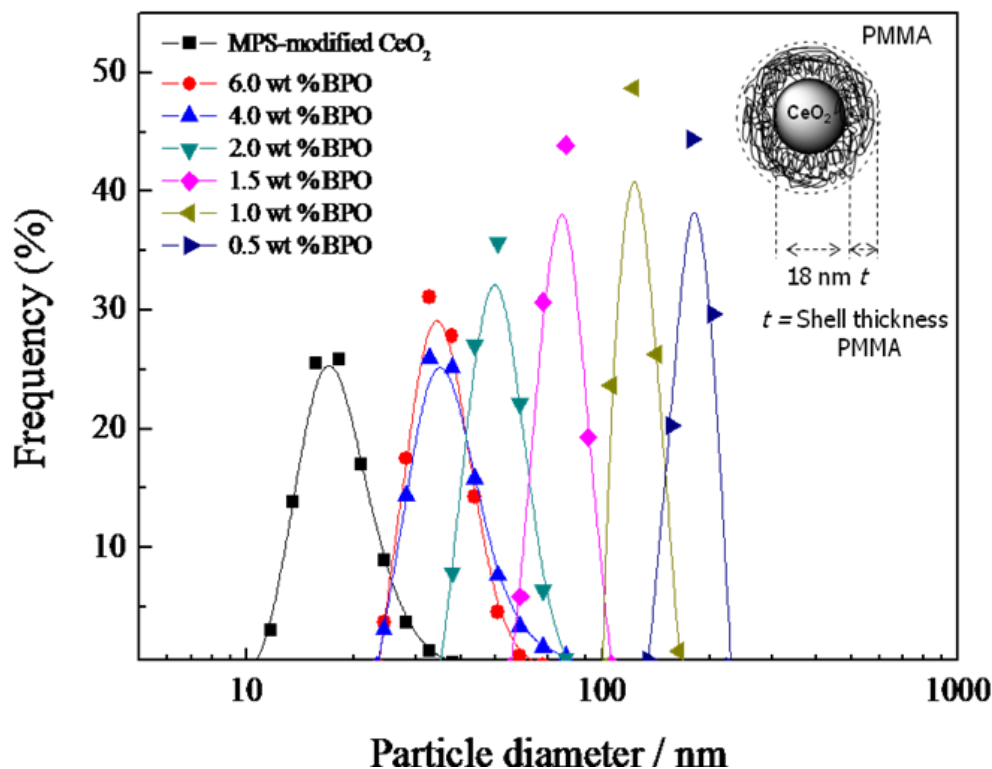
Figure 2.6. DLS number size distribution of $CeO_2$ core and PMMA-grafted $CeO_2$ particles at varying shell thickness in toluene.

It was previously shown that the particles in polymerization medium interfere with the polymerization process.(Demir, et al. 2007a; Demir, et al. 2006; Kashiwagi, et al. 2003) The in situ formed polymer chains are in general longer compared to the chains obtained in the absence of nanoparticles. To make a rough estimation about the molecular weight obtained on the surface of particles, polymerization was carried out in absence of particles using the same conditions (temperature, time, solvent, and initiator content) employed in the process of in situ polymerization. The results of the experiments are given on right y-axis of Figure 2.7. As expected, an inverse relationship takes place between the molecular weight and the initiator content. For a typical free radical polymerization, it is well-known that initiator amount is inversely proportional with the square root of kinetic chain length of polymer chain obtained.(Odian) At a fixed amount of monomer, increasing concentration of initiator leads to formation of smaller chains. Thus, a similar relationship between the amount of initiator and $t$ was observed in our particular example. The higher the BPO content, the shorter the PMMA thickness is. The diameter of PMMA coil in toluene (a good solvent) can be estimated from the Flory's meanfield approach:(Flory 1953)

$$R_g = N^{3/5} \, l \qquad\qquad\qquad (2.1)$$

where $R_g$ is radius of gyration that is average distance from the center of the gravity to the chain segment. $N$ is degree of polymerization, and $l$ is the length of C-C bond in monomer (1.5 Å). Based on this calculation, it is obvious that the thickness of PMMA is longer than the size of an average chain. For example, the diameter of a PMMA coil is 10 nm when the BPO content was 1.5 wt %. At the same BPO content, the thickness of the shell is 29 nm. This result indicates the existence of multilayer grafting of PMMA chains on the surface of $CeO_2$ core. In the first layer, PMMA chains are chemically linked to the surface of the particles through MPS from one may be more than one molecule. In the second layer, the chains are physically adsorbed to the first layer. This process occurs several times layer-by-layer radially outward from the surface of particles and eventually forms a homogeneous coating around each particle, called bound polymer. Note that the chains adsorbed onto the surface via mainly physical means; however, the detachment of the chains was not observed. The dispersion of hybrid particles was stable such that the same particle size distribution was obtained from the hybrid particles even after 1 week stay in the shelves.
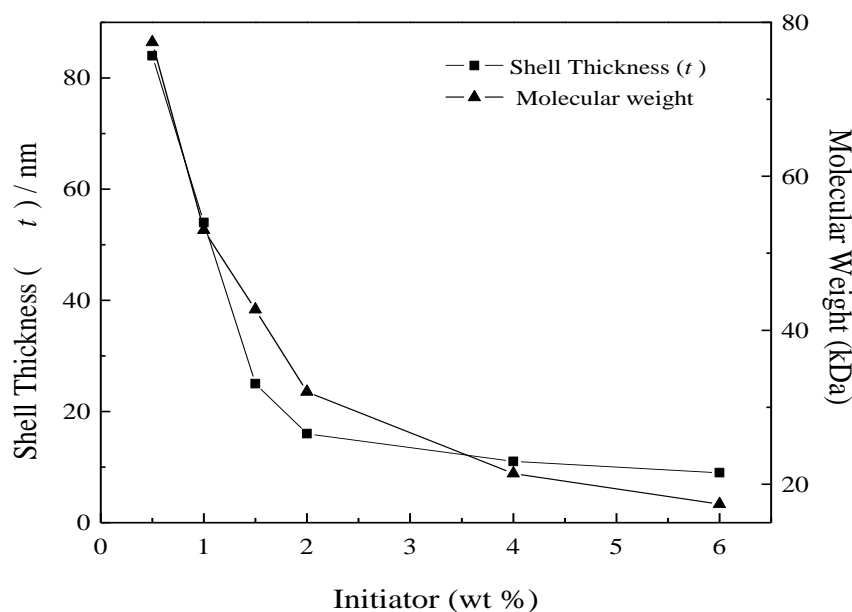


Figure 2.7. The thickness of PMMA shell and molecular weight of PMMA prepared in the absence of particles as a function of initiator (BPO) content.

Figure 2.8. depicts typical powder X-ray diffraction (XRD) patterns of unmodified, MPS-modified and PMMA-grafted $CeO_2$ nanoparticles. The patterns show chracteristic diffractions of $CeO_2$. All diffraction peaks of $CeO_2$ nanoparticles correspond to a cubic flourite structure (JCPDS-34-0394) and they can be indexed as (111), (200), (220), (311), (400) and (331). After MPS-modification of particles, all diffractions of particles are avoided. However, XRD pattern of PMMA-grafted particles is smoother than other patterns. It is known that crystallinity of polymers is amorphous and grafted polymers suppress chracteristic peaks of $CeO_2$.

Crystallite size of the particles was determined from the line broadening of the (111) reflection of the XRD pattern using Scherrer's formula:

$$L = \frac{\alpha\lambda}{BCos\ \theta_b}$$

(2.2)

where $L$ is the mean particle size, $\alpha$ is a geometric factor equal to 0.94, $\lambda$ is the X-ray wavelength (1.542 Å), and $\beta$ is the half-width of the diffraction peak. The size of the crystallite particles was found to be 15.7 nm for the unmodified $CeO_2$ particles.



Figure 2.8. Powder X-ray diffraction spectra of unmodified, MPS-modified and PMMA-grafted $CeO_2$ particles.

A drop of PMMA-grafted $CeO_2$ dispersion was cast on TEM grid from toluene. After evaporation of solvent, the surface is examined by TEM. Figure 2.9. shows TEM images of MPS modified and PMMA-grafted $CeO_2$ particles. Panel a shows representative overview image of MPS-modified $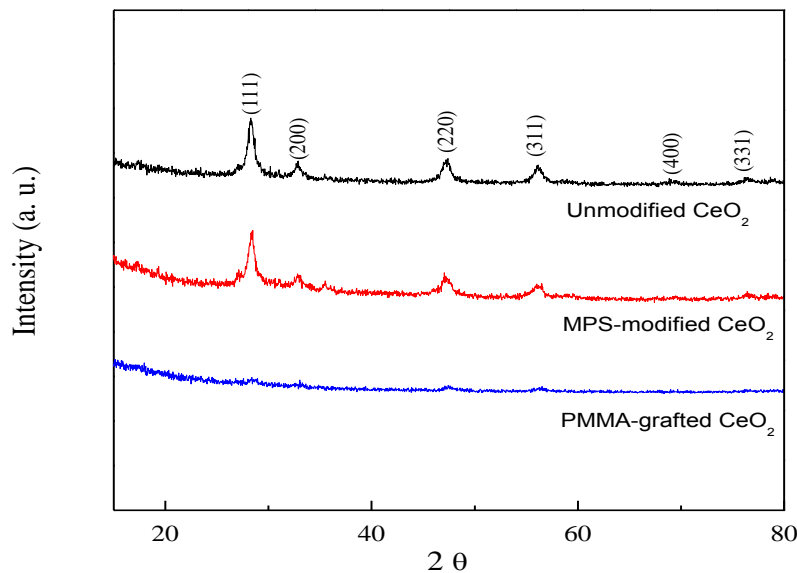CeO_2$ particles in well-dispersed state. The particles are spherical and uniform size. The average particle diameter measured from 100 particles was about $18 \pm 8$ nm, that is consistent with the size measured by DLS ($d = 18$ nm). While the MPS-modified $CeO_2$ particles are well separated on carbon film of the TEM grid, the PMMA-grafted $CeO_2$ particles appeared in clusters. The adhesive interaction between the PMMA segments of neighboring PMMA-grafted $CeO_2$ particles leads to formation of clusters. The core $CeO_2$ particles are evident in the clusters. Although the entire population of core-shell particles is individually dispersed in toluene depending on DLS measurements, the colloidal nanocomposites adhere each other due to solvent evaporation.
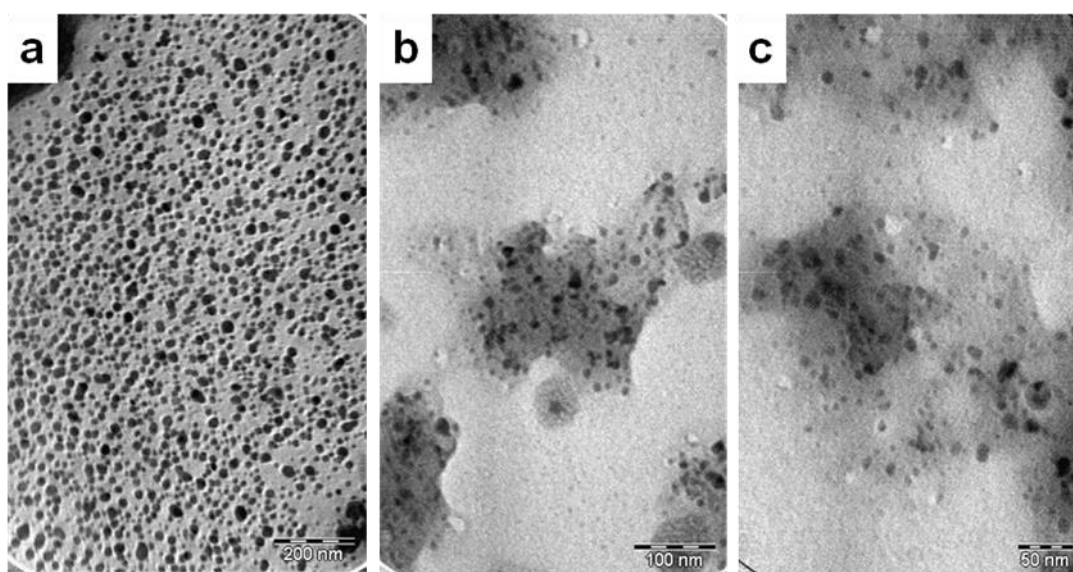


Figure 2.9. TEM images obtained from (a) as-synthesized $CeO_2$, (b) PMMA-grafted $CeO_2$ particles with 16 nm PMMA thickness, and (c) PMMA-grafted $CeO_2$ particle with 29 nm PMMA thickness.

The corresponding MPS-modified $CeO_2$, and unmodified $CeO_2$, and PMMA-grafted $CeO_2$ particles with varying thicknesses were characterized by TGA (Figure 2.10.). Below 300 °C, mass loss of nearly 4 wt % takes place due to loss of absorbed water and dehydration of silane groups on particle surface. A sharp mass loss was observed from 300 to 400 °C owing to the thermal oxidation and decomposition of

polymer layer grafted onto the CeO$_2$ particles. As a result of disappearance of polymeric residue, the mass stays almost unchanged above 400 °C. The remaining mass refers to inorganic residue mainly composed of CeO$_2$ particles. Therefore, the percent mass loss above this temperature hint about the amount of PMMA layer on ceria particles. Considering that the size of CeO$_2$ particles remains unchanged at 18 nm, the PMMA-grafted nanocomposite particles that have longer shell thickness should undergo higher amount of mass loss, this is in fact what we have observed in this thermogram. The mass loss originated from PMMA on the particle surface were found as 73, 75, and 93 wt % for the core-shell particles having 9 nm, 11 nm, and 16 nm shell thicknesses, respectively.



Figure 2.10. TGA curves for unmodified, MPS-modified and PMMA-grafted CeO$_2$ particles.

Table 2.1 Theoretical and measured mass ratio of PMMA shell to the particle core. (Theoretical calculations were made by assuming each particle size as 18nm, measured data by obtained after TGA measurements )
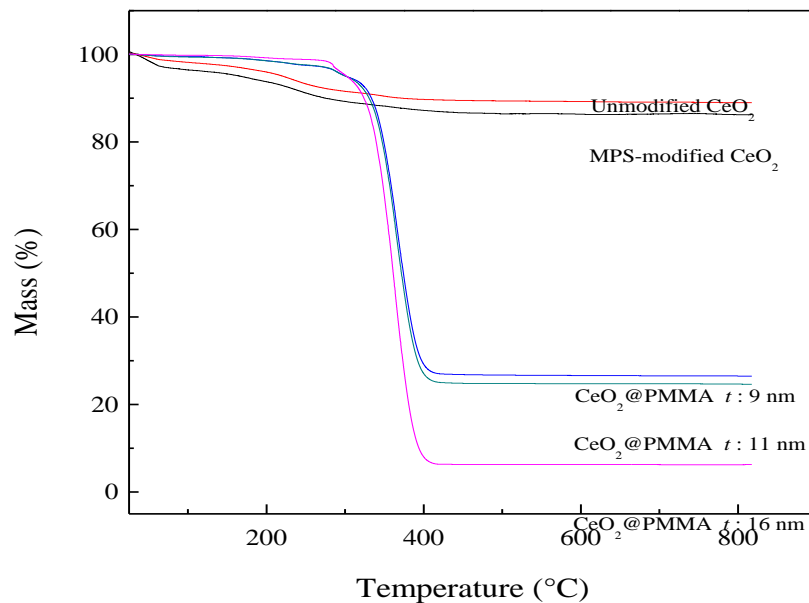
| Sample | Theoretical ($m_{shell}/m_{core}$) | Measured ($m_{shell}/m_{core}$) |
|---|---|---|
| Unmodified $CeO_2$ | - | - |
| MPS-modified $CeO_2$ | - | - |
| $t$ : 9 nm | 1.3 | 2.6 |
| $t$ : 11 nm | 1.5 | 3 |
| $t$ : 16 nm | 7 | 13 |
| $t$ : 29 nm | 11 | 24 |
| $t$ : 54 nm | 50 | 26 |
| $t$ : 84 nm | 140 | 34.7 |

The grafting of both MPS and PMMA on the surface of core ceria nanoparticles was validated by vibrational spectroscopy. FTIR spectra of unmodified $CeO_2$, MPS-modified $CeO_2$, and PMMA-grafted $CeO_2$ nanoparticles are shown in Figure 2.11. The strong absorption band at 1384 $cm^{-1}$ is present at all three spectra regardless of the chemical grafting on the particle surface. This band is attributed to the surface adsorbed nitrate groups coming from the unreacted $Ce(NO_3)_3 \cdot 6H_2O$.(Hashimoto, et al. 2000; Xu, et al. 2008) Upon surface treatment of the particles with MPS, three major signals at 1722 $cm^{-1}$, 1638 $cm^{-1}$ and 1193-1168 $cm^{-1}$ appear in the spectrum as a result of C=O stretching, C=C stretching, and ester vibration (C-O-C), respectively. We observed that the signals of adsorbed groups are remarkably broader compared to the one of fresh MPS. Moreover, the spectrum of MPS-modified $CeO_2$ particles shows some of new bands in the range of 800-1000 $cm^{-1}$ other than signals of fresh MPS. These bands are originated from Ce-O-Si bond indicating hydrolysis of hydroxyl groups on $CeO_2$ surface with silanol groups of MPS and succesful chemical grafting of MPS onto particle surface. After polymerization of MMA and MPS on particle surface, the shape of the spectra is strongly altered. The spectral feature is almost disappeared. The signals are broadened and intensity of signals is remarkably reduced. The finger print signal of carbonyl group at 1722 $cm^{-1}$ and 1600 $cm^{-1}$ are evident in the spectra. The characteristic signals of PMMA chain

overcome the signals of MPS and $CeO_2$, the surface of particles is fully covered with PMMA chains.
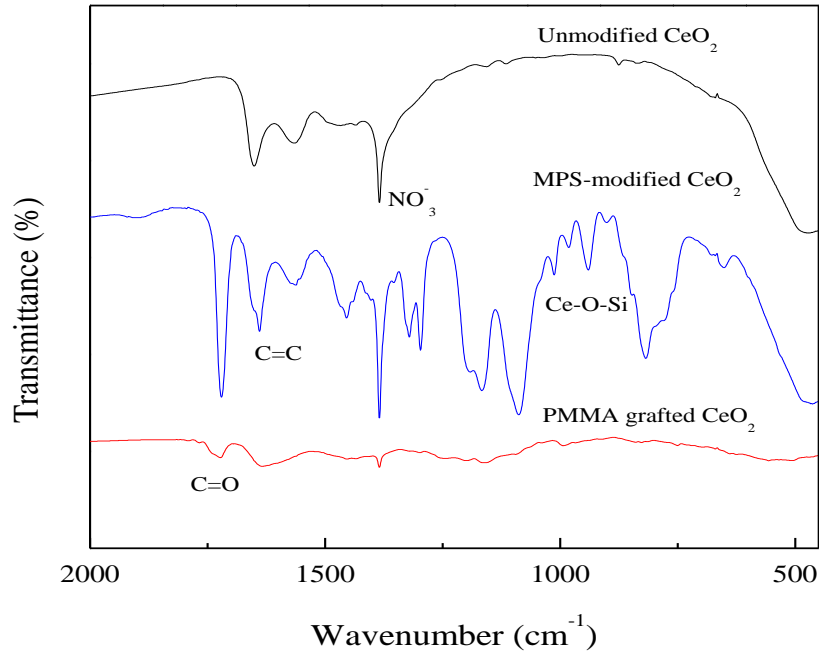


Figure 2.11. FT-IR spectra of unmodified, MPS-modified and PMMA-grafted $CeO_2$ particles.

## 2.2.3. Preparation of PS / PMMA-grafted $CeO_2$

A series of nanocomposites was prepared by blending of PS / THF solution (20.0 wt % PS) with neat $CeO_2$ particles, MPS-modified $CeO_2$ particles, and PMMA-grafted $CeO_2$ particles with different shell thicknesses. The composite films were carefully examined by AFM to figure out the dispersion of PMMA-grafted $CeO_2$ particles in PS matrix. Figure 2.12. shows AFM tapping mode phase images of PS matrix loaded with PMMA-grafted $CeO_2$ particles with different PMMA shell thickness. In fact, PS and PMMA are two dissimilar polymers that undergo macrophase separation.(Helfand and Tagami 1972) Since PMMA chains are chemically grafted onto the surface of $CeO_2$ particles in our system, macrophase separation is not observed. In AFM, a sharp tip slides across the surface to gain information. The interaction of the tip is limited with the outer topmost layer of a specimen. The bright regions in the images

refer to PMMA layer present on the $CeO_2$ particles so that the $CeO_2$ core cannot be resolved from the images. The average diameter of the PMMA-grafted $CeO_2$ particles observed by AFM is compared with the mean diameter of particles measured by DLS. The results are given in Table 1. For example, in panel a, the diameter of particles was found as $134\pm100$ nm measured from at least 20 particles. The mean diameter of particles was measured as 126 nm by DLS. In Panel b, the diameter of these particles was found as $57\pm19$ nm whereas the mean diameter of these particles was found as 76 nm in DLS measurement. The consistency of the results obtained by AFM and DLS indicates that the PMMA-grafted $CeO_2$ particles are dispersed into PS matrix individually and free of remarkable aggregates.
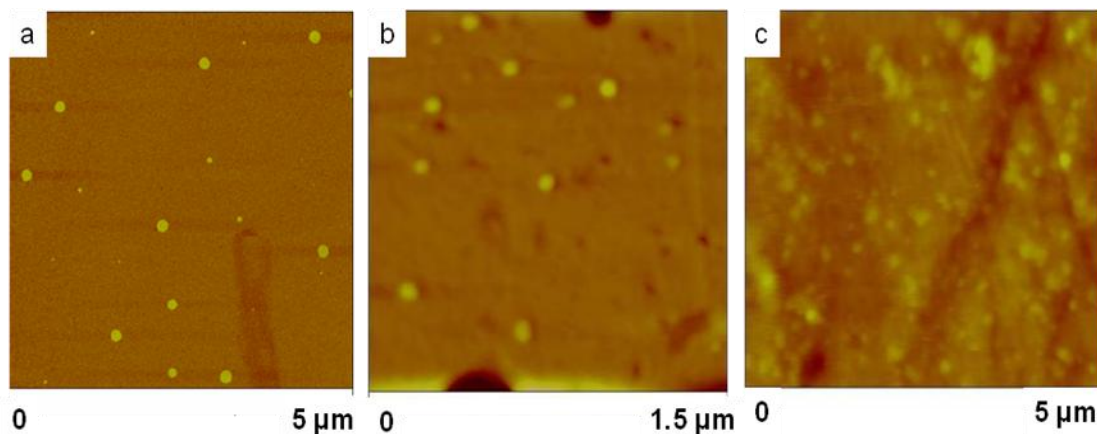


Figure 2.12. AFM images of the PMMA-grafted $CeO_2$ particles having 54 nm (a), 29nm (b), 9 nm (c) shell thickness particles in PS.

## 2.2.4. Transmission of the Composite Films.

The nanocomposites were spin-coat on quartz glass and transmission of these films was examined over UV-visible region. Figure 2.13. shows the UV-vis transmission spectra of both neat PS and PS based composite films prepared with unmodified, MPS-modified, or PMMA-grafted $CeO_2$ particles. In all composite films, the $CeO_2$ content was fixed to 5.5 wt %. The films are non-absorbing over visible region. Neat PS has the highest transmission value among all composite films. The intensity loss at this region is mainly due to the scattering of ceria particles. On the other hand, the films are absorbing at UV region of the spectrum. This behavior is not a surprise since both ceria and styrene groups in PS matrix are absorbing in this region.

Ceria is a semiconductor having 3.3 eV band-gap energy, which is comparable with the energy of UV region. So that it is absorbing material particularly at UV-A region (290-200 nm). In addition, styrene involves a benzene group that is particularly encountered by the UV radiation. In these spectra, we mainly focus on the visible region where we can compare the intensity loss due to scattering at particular PS/ceria composite system. Since human eye has the highest sensitivity at 550 nm, the spectra of nanocomposites were compared with respect to their transmission at this wavelength.
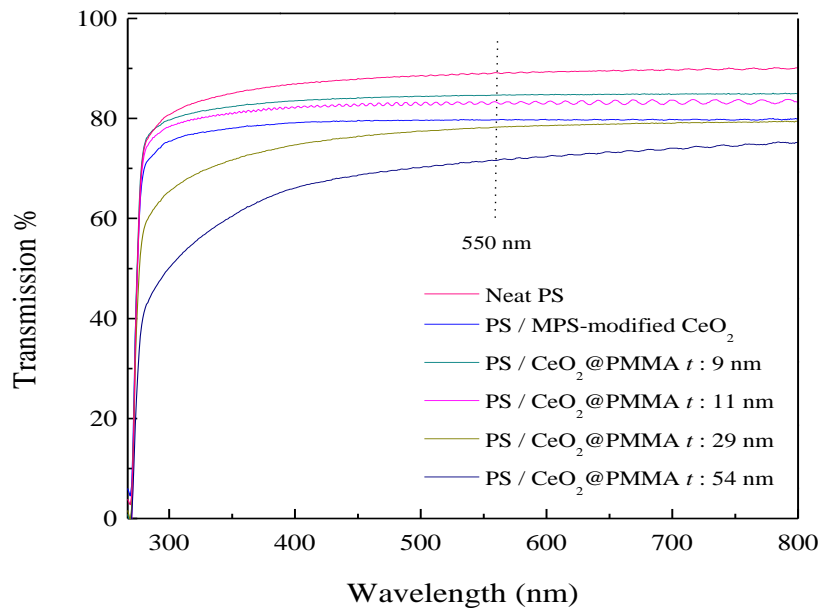


Figure 2.13. UV-vis transmission spectra of the neat PS and the PMMA-grafted $CeO_2$ particles at varying shell thickness in PS matrix.

Transmission of all PS/$CeO_2$ nanoparticle composites prepared by PMMA-grafted $CeO_2$ particles as a function of PMMA shell thickness is given on Figure 2.14. Neat PS has ~90 % transmission at normal incidence. This result is consistent the information given in literature.(Tu, et al. 2010) The incorporation of unmodified particles into PS matrix causes more than 20 % loss in transmission. AFM measurements showed that (not shown) the particles are not dispersed well into PS matrix forming large particle domains that cause scattering and accordingly intensity loss. The modification of MPS improves the dispersion of particles and therefore transmission of the composite film. On the other hand, the transmission of PS nanocomposites prepared by PMMA-grafted $CeO_2$ particles depends on the thickness of PMMA. At the same ceria content, the transmission increases up to a value of 85 %

when the polymer shell thickness is 9 nm. The increase of shell thickness from 9 nm to 29 results a decrease in transmission. Further increase in thickness of the polymer shell results a dramatic loss of transparency of the composites.
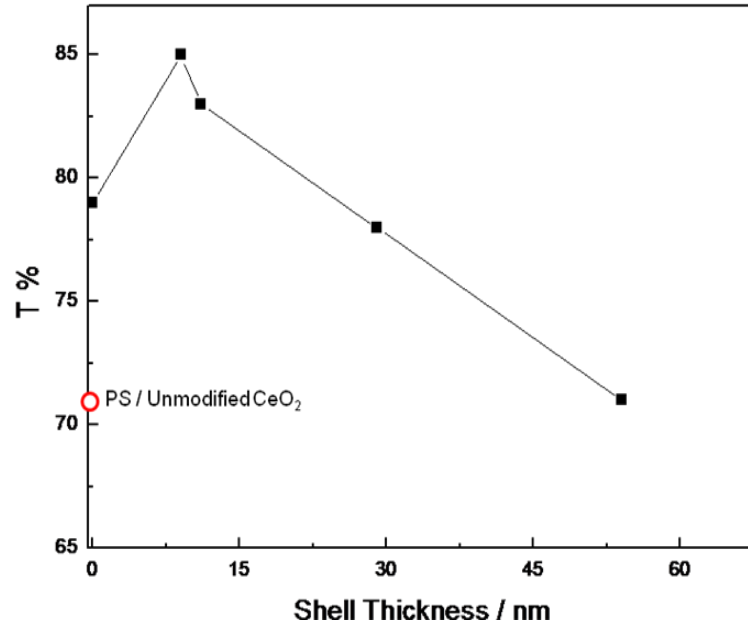


Figure 2.14. Transmission values of the PS / PMMA-grafted $CeO_2$ nanocomposites at 550 nm. The data points were obtained from the transmission spectra of the composite films in Figure 2.12.

The highest transparency among all composite films is obtained from the nanocomposites prepared particles whose shell thickness is 9 nm. At this thickness, scattering is remarkably minimized most probably due to the index matching between RI of particles with that of surrounding PS matrix. The refractive index of overall composite system can be estimated by Maxwell-Garnett formula. It can also be applied to our colloidal nanocomposite system.

According to this theory, scattering which is originated from the presence of high refractive index particle will be diminished if the effective dielectric constant of the core-shell particle equals to the one of the embedding medium ($\varepsilon_{effective} = \varepsilon_{medium}$).

Depending on the Maxwell-Garnett formula (eq. 5), for a given ceria nanoparticles with 18 nm in diameter, shell thickness of $CeO_2$ for index matching condition is 7 nm. The increase in PMMA content at a fixed amount of ceria core

26

lowers the refractive index of overall PMMA-grafted $CeO_2$ particles. In other words, at longer PMMA thickness the refractive index of PMMA-grafted $CeO_2$ particle as a separate system decreases even lower than that of PS matrix, which develops another source of RI mismatch and therefore optical scattering.
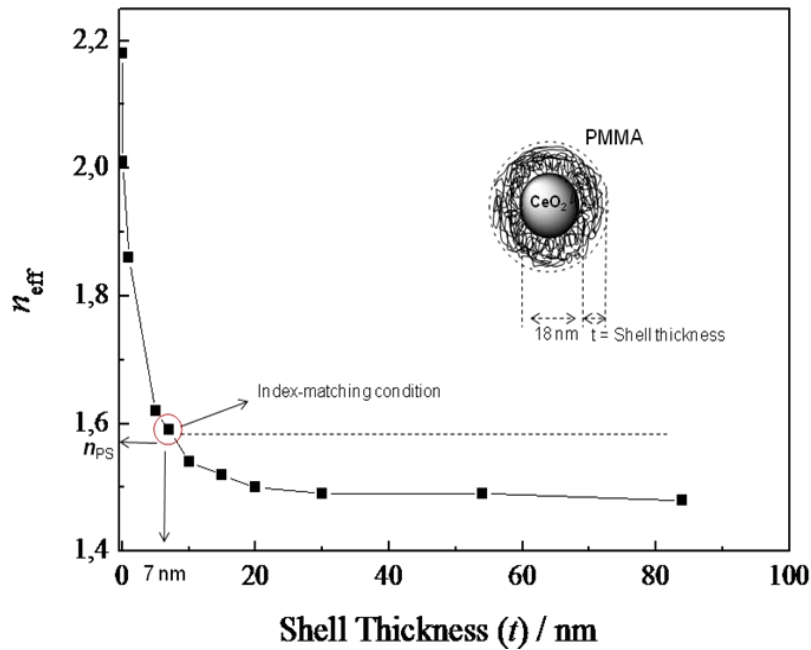


Figure 2.15. Effective refractive index of $CeO_2$@PMMA core-shell particles as a function of shell thickness calculated using Equation 5 and assuming $n_{CeO2}= 2.18$, $n_{PMMA}= 1.489$ for the refractive index of $CeO_2$ and PMMA, respectively. The dotted line represents the refractive index of PS ($n_{PS}= 1.589$). At the 7 nm thickness on surface, particles are predicted to be index-matched to the PS.

The blend film of PS and PMMA without $CeO_2$ particles were prepared for the reason of comparison. The amount of PMMA was used as the exact amount of PMMA employed in PMMA-grafted $CeO_2$. The transmission of this blend film was found as 67 % at this wavelength. A strong phase separation of PMMA in PS matrix is validated by tapping mode AFM. This result underlines the importance of material composition for index matching process. The usage of PMMA and PS without ceria nanoparticles does not make sense, rather, lowers the transmission even lower than the one of unmodified ceria nanoparticles.
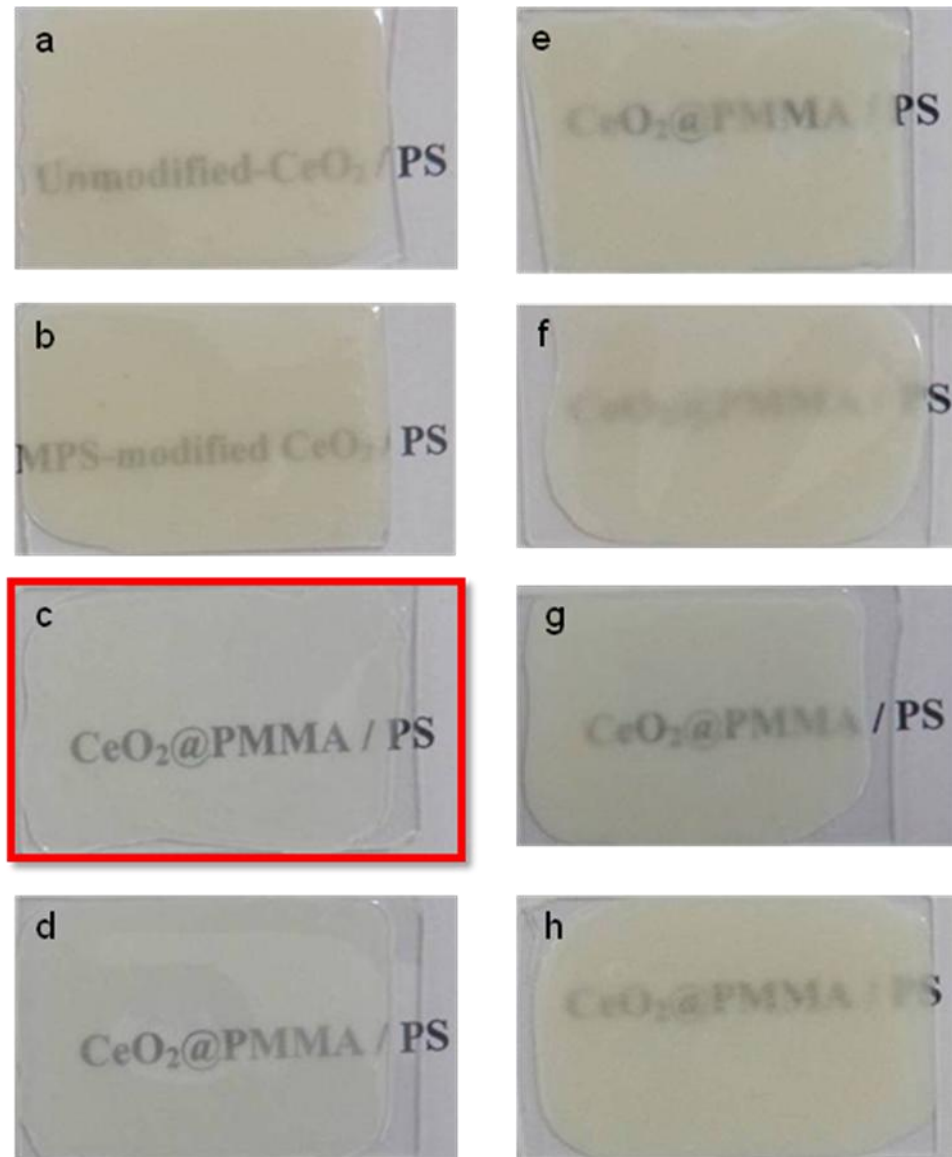
Figure 2.16. Photo of the nanocomposites film prepared by casting. The thickness of the films is around 2.5 μm. The amount of $CeO_2$ was fixed to 5 wt %. **a)** PS/unmodified $CeO_2$ particles **b)** PS/MPS modified $CeO_2$ particles **c)** PS/PMMA-grafted $CeO_2$ particles, $t = 9$ nm **d)** PS/PMMA-grafted $CeO_2$ particles, $t = 11$ nm **e)** PS/PMMA-grafted $CeO_2$ particles, $t = 16$ nm **f)** PS/PMMA-grafted $CeO_2$ particles, $t = 29$ nm **g)** PS/PMMA-grafted $CeO_2$ particles, $t = 54$ nm **h)** PS/PMMA-grafted $CeO_2$ particles, $t = 84$ nm.

The achievement of transparency in PS nanocomposites can be readily seen by naked eyes on thicker films. Figure 2.16 shows the photographic images of the films cast from THF with 350 μm on average. The composite films prepared by unmodified and MPS-modified particles have strong opacity (a,b). However, an obvious recruitment in transmission is observed for the composite containing colloidal nanocomposite that has 9 nm PMMA shell thickness (c). This composite is the one where we believe that

28

index-matching condition is provided. The increase of polymer shell thickness on particle core results translucency. At the longest the longest thickness, the composite exhibit strong opacity. Thus, photographic images of all composite films are in accordance with UV-visible transmittance for these composites, and same trend in transparency loss can be attained.

Table 2.2. Mean diameter and polydispersity index (PDI) of particle size distribution (PSD) of PMMA-grafted $CeO_2$ particles and average diameter of the particle domains at different amount of BPO initiator.

| Sample | Mean of PSD of PMMA-grafted $CeO_2$ particles obtained by DLS / nm | PDI of PSD obtained by DLS | Average diameter of PMMA-grafted $CeO_2$ particle domains obtained by AFM (nm) |
|---|---|---|---|
| $CeO_2$@PMMA (BPO 6.0 wt %) | 36 | 0.4 | $30 \pm 12$ |
| $CeO_2$@PMMA (BPO 4.0 wt %) | 40 | 0.4 | $45 \pm 15$ |
| $CeO_2$@PMMA (BPO 2.0 wt %) | 51 | 0.3 | $90 \pm 14$ |
| $CeO_2$@PMMA (BPO 1.5 wt %) | 76 | 0.4 | $57 \pm 19$ |
| $CeO_2$@PMMA (BPO 1.0 wt %) | 126 | 0.3 | $134 \pm 100$ |
| $CeO_2$@PMMA (BPO 0.5 wt %) | 187 | 0.3 | $236 \pm 60$ |

# CHAPTER 3

# CONCLUSION

We demonstrated that transparency of a composite system can be remarkably increased when refractive index difference is minimized between particles and surrounding polymer matrix. The association of PS and unmodified $CeO_2$ particles results an opaque material due to the both aggregation of particles and RI mismatch. Well-defined PMMA-grafted $CeO_2$ colloidal particles with different thickness of PMMA layer were successfully synthesized using combination of controlled precipitation of $CeO_2$ nanoparticles and free radical in situ solution polymerization of MMA. The thickness of PMMA on the particle surface was readily controlled by the amount of BPO. The colloidal PMMA-grafted $CeO_2$ nanoparticles were also blended with PS matrix and the thickness was found to be an important parameter for the transparency of the ternary composite. We demonstrated that when the refractive index of PMMA-grafted $CeO_2$ particles matches the refractive index of embedded PS medium, a quasi-transparent nanocomposite film is formed due to the reduction of refractive index difference between the particles and surrounding medium. This approach can be successfully applied for transparency of all heterogeneous structures not only for visible light but also for different segments of optical spectrum.

# REFERENCES

Advincula, R. 2006. Polymer brushes by anionic and cationic Surface-Initiated Polymerization (SIP). *In* Surface-Initiated Polymerization I. Pp. 107-136. Advances in Polymer Science.

Asunskis, D. J., I. L. Bolotin, and L. Hanley. 2008. Nonlinear optical properties of PbS nanocrystals grown in polymer solutions. *Journal of Physical Chemistry C* 112:9555-9558.

Baekeland, L. H. 1909. Sci. Am. (68):322.

Balazs, A. C., T. Emrick, and T. P. Russell. 2006. Nanoparticle polymer composites: Where two small worlds meet. *Science* 314:1107-1110.

Beecroft, L. L., and C. K. Ober. 1997. Nanocomposite materials for optical applications. *Chemistry of Materials* 9:1302-1317.

Bockstaller, M. R., R. A. Mickiewicz, and E. L. Thomas. 2005. Block copolymer nanocomposites: Perspectives for tailored functional materials. *Advanced Materials* 17:1331-1349.

Bombalski, L., et al. 2007. Null-scattering hybrid particles using controlled radical polymerization. *Advanced Materials* 19(24):4486.

C.F. Bohren, D.R. Hoffman. 1983. *In Absorption and Scattering of Light by Small Particles*. New York: Wiley.

Caseri, W. 2009. Inorganic Nanoparticles as Optically Effective Additives for Polymers. *Chemical Engineering Communications* 196(5):549-572.

Caseri, W. R. 2006. Nanocomposites of polymers and inorganic particles: preparation, structure and properties. *Materials Science and Technology* 22:807-817.

Chang, C. C., and W. C. Chen. 2002. Synthesis and optical properties of polyimide-silica hybrid thin films. *Chemistry of Materials* 14:4242-4248.

D.N., Dimitriev V.G.; Gurzadyan G.G.; Nikogosyan. *Handbook of Nonlinear Optical Crystals*: Springer; 2nd Rev. Ed.

Demir, M. M., et al. 2007a. In-situ bulk polymerization of dilute Particle/MMA dispersions. Macromolecules 40:4190-4198.

Demir, M. M., et al. 2007b. Optical properties of composites of PMMA and surface-modified zincite nanoparticles. *Macromolecules* 40:1089-1100.

Demir, M. M., et al. 2006. PMMA/zinc oxide nanocomposites prepared by in-situ bulk polymerization. *Macromolecular Rapid Communications* 27:763-770.

Devaraju, N. G., E. S. Kim, and B. I. Lee. 2005. The synthesis and dielectric study of BaTiO3/polyimide nanocomposite films. *Microelectronic Engineering* 82:71-83.

Du, H., et al. 2002. Synthesis, characterization, and nonlinear optical properties of hybridized CdS-polystyrene nanocomposites. *Chemistry of Materials* 14:4473-4479.

Elim, H. I., et al. 2003. Ultrafast optical nonlinearity in poly(methylmethacrylate)-TiO2 nanocomposites. *Applied Physics Letters* 82:2691-2693.

Feng, M., et al. 2009. CdS nanoparticles chemically modified PAN functional materials: Preparation and nonlinear optical properties. *European Polymer Journal* 45:1058-1064.

Flory, Paul J. 1953. Principles of Polymer Chemistry. Ithaca and London: Cornell University Press.

Goodyear, Charles. 1856. Dinglers Polytechnisches Journal (139):376.

Hashimoto, K., et al. 2000. Photocatalytic oxidation of nitrogen monoxide over titanium(IV) oxide nanocrystals large size areas. *Journal of Photochemistry and Photobiology a-Chemistry* 136:103-109.

Helfand, E., and Y. Tagami. 1972. Theory of Interface Between Immiscible Polymers. 2. *Journal of Chemical Physics* 56:3592.

Hu, Y. Q., S. X. Zhou, and L. M. Wu. 2009. Surface mechanical properties of transparent poly(methyl methacrylate)/zirconia nanocomposites prepared by in situ bulk polymerization. *Polymer* 50:3609-3616.

Hulst, H. C. v. d., ed. *Light Scattering by Small Particles*: Dover Publications, New York 1981.

Hung, C. H., and W. T. Whang. 2005. Effect of surface stabilization of nanoparticles on luminescent characteristics in ZnO/poly(hydroxyethyl methacrylate) nanohybrid films. *Journal of Materials Chemistry* 15:267-274.

J. C. Seferis in : J. Brandrup, E. H. Immergut, E. A. Grulke (Eds.) "Polymer Handbook", 4th ed., Wiley, New York, 1999, p. 6/578

Kashiwagi, T., et al. 2003. Thermal and flammability properties of a silica-poly(methylmethacrylate) nanocomposite. *Journal of Applied Polymer Science* 89:2072-2078.

Khanna, P. K., and N. Singh. 2007. Light emitting CdS quantum dots in PMMA: Synthesis and optical studies. *Journal of Luminescence* 127:474-482.

Kohlmann, O., et al. 2001. NMR diffusion, relaxation, and spectroscopic studies of water soluble, monolayer-protected gold nanoclusters. *Journal of Physical Chemistry B* 105:8801-8809.

Kojma, Y. 1993. *Journal of Material Research* 8:1185.

Kulyk, B., et al. 2009. Linear and nonlinear optical properties of ZnO/PMMA nanocomposite films. *Journal of Applied Physics* 106:6.

Li, Y. Q., et al. 2008. Facile synthesis of highly transparent polymer nanocomposites by introduction of core-shell structured nanoparticles. *Chemistry of Materials* 20:2637 2643.

Lu, C. L., and B. Yang. 2009. High refractive index organic-inorganic nanocomposites: design, synthesis and application. *Journal of Materials Chemistry* 19:2884-2901.

Novak, B. M. 1993. Hybrid Nanocomposites Materials- between Inorganic Glasses and Inorganic Glasses and Organic Polymers. *Advanced Materials* 5:422-433.

Nussbaumer, R. J., et al. 2003. Polymer-TiO2 nanocomposites: A route towards visually transparent broadband UV filters and high refractive index materials. *Macromolecular Materials and Engineering* 288:44-49.

Odian, George. *Principles of Polymerization*: Wiley-Interscience, 4th ed.

Palkovits, R., et al. 2005. Polymerization of w/o microemulsions for the preparation of transparent SiO2/PMMA nanocomposites. *Langmuir* 21:6048-6053.

Qi, H., and T. Hegmann. 2008. Impact of nanoscale particles and carbon nanotubes on current and future generations of liquid crystal displays. *Journal of Materials Chemistry* 18:3288-3294.

Schulz, H., P. Burtscher, and L. Madler. 2007. Correlating filler transparency with inorganic/polymer composite transparency. *Composites Part a-Applied Science and Manufacturing* 38:2451-2459.

Schulz, H., et al. 2005. Transparent nanocomposites of radiopaque, flame-made Ta2O5/SiO2 particles in an acrylic matrix. *Advanced Functional Materials* 15:830-837.

Talapin, D. V., et al. 2010. Prospects of Colloidal Nanocrystals for Electronic and Optoelectronic Applications. *Chemical Reviews* 110:389-458.

Tu, Y., et al. 2010. Transparent and flexible thin films of ZnO-polystyrene nanocomposite for UV-shielding applications. *Journal of Materials Chemistry* 20:1594-1599.

Xu, J. X., L. P. Li, and G. S. Li. 2008. A facile approach to well-dispersible CeO2 nanoparticles. *Journal of Dispersion Science and Technology* 29:1072-1076.

Yamada, N., I. Yoshinaga, and S. Katayama. 1999. Processing and optical properties of patternable inorganic-organic hybrid films. *Journal of Applied Physics* 85:2423-2427.

Yang, Y., et al. 2008. Transparent and light-emitting epoxy nanocomposites containing ZnO quantum dots as encapsulating materials for solid state lighting. *Journal of Physical Chemistry C* 112:10553-10558.

Yoshida, M., and P. N. Prasad. 1996. Sol-gel-proceseed SiO2/TiO2/poly (vinylpyrrolidone) composite materials for optical waveguides. *Chemistry of Materials* 8:235-241.

Yuwono, A. H., et al. 2006. Titania-PMMA nanohybrids of enhanced nanocrystallinity. *Journal of Electroceramics* 16:431-439.

Zhang, F., Q. Jin, and S. W. Chan. 2004. Ceria nanoparticles: Size, size distribution, and shape. *Journal of Applied Physics* 95:4319-4326.

Zhang, H., et al. 2003. From water-soluble CdTe nanocrystals to fluorescent nanocrystal-polymer transparent composites using polymerizable surfactants. *Advanced Materials* 15:777.